DESIGN AND DEVELOPMENT OF NANOSENSORS BASED SOIL CONDITION MONITORING SYSTEM WITH IOT TECHNOLOGY

Synopsis submitted in fulfilment of the requirements for the degree of

Doctor of Philosophy

In

Electronics

By

AKSHAYA KUMAR A

Under the Guidance of

Dr. NAVEEN KUMAR S K

Professor

Department of Studies and Research in Electronics

Mangalore University

Mangalagangothri-574199, India

March 2022

Synopsis of the Doctoral Thesis

Name of the student	Akshaya Kumar A
Name of the research guide	Dr. Naveen Kumar S K
Title of Ph.D. thesis	Design and Development of Nanosensors Based Soil Condition Monitoring System with IoT Technology
Workplace	Department of Studies and Research in Electronics, Mangalore University, Mangalagangothri, Konaje-574199.
Date of registration	27/02/2017
Ph.D. registration number	No. MU/EXB/Ph.D. / CR.26/Ele./ 2018-19/ E.13 dated 26.06.2018
Nature of registration	Full Time
Subject	Electronics
Faculty	Science and Technology

1. BACKGROUND AND MOTIVATION OF THE STUDY

Human beings' lives are either directly or indirectly reliant on agricultural activities.[1]. In concern of supplying food to the exponentially growing population in the world [2], there has to be modern technology is required in agriculture that will enhance the crop production from the available agricultural land. One of the most crucial factors which affect agricultural production is soil fertility conditions[3]. However, excessive chemical fertilizers and pesticides are added to the soil without knowing its specific requirement to increase crop production. This unnecessary addition of fertilizers and pesticides contaminates the surface of soil and groundwater, which causes an undesirable environmental impact and a disproportionate increase in the cost of production. Thus, real-time checking and controlling of soil conditions before, after, and display plays a significant role in agricultural crop yield and supports smart farming practices. Soil is the essential element of agriculture and production of crop yield directly depending on the soil physicochemical conditions[4][5][6][7]. Considering the importance of soil condition level detection, cost-effective, reliable, user-friendly, and eco-friendly, disposable multifunctional soil condition sensing devices are highly demanded. It covers many application areas like digital agriculture, wastewater management, and environmental applications[8]. But farmers and most of the agricultural industries follow the traditional approaches to track soil conditions[9][10][11][12]. These detection methods have suffered from many challenges, and these conventional approaches have to be replaced by modern technology.

Nitrogen (N) is an essential element for plant growth and a limiting factor in terrestrial ecosystems, and plants can directly take up Ammonium (NH_4^+) from the soil. The soil pH level controls the physical, chemical, and biological processes of NH_4^+ holding and supplying capacity; it is best soluble and bio-available at pH values in-between 5.5 and 6.5. However, soil analytes have many interferants in a wide window of ionic and pH concentration levels in the soil. Many of the available pH and NH_4^+ sensor electrode platforms foul with electrochemical conditions, and all these lead to inaccurate sensor results. The sensors used today in agriculture systems are often nondegradable. Those sensors are inserted into the agriculture field have the disadvantages of extractions of the sensor platforms after its use, which become an additional burden for the farmers.

Great efforts are being made to find new ways of producing interconnected disposable electrochemical sensor systems on a real-time agricultural field to resolve the extractions of the sensor platforms. A novel method of nanomaterial-based electrochemical sensor platforms fabrication coupled with Machine Learning (ML) approaches drives the eco-friendly intelligence system for digital agriculture. It can cut down sensor optimization cost and time, provide unexpected insights into the experimental data, predict the outcome by deciphering non-linear analytical input signals without mathematical fitting, readily integrated into an IoT setting. The ability for real-time soil conditions would expressively improve the data about the fertilizer and pH conditions required for the healthy growth of plants and their production.

2. SCOPE OF THE PRESENT WORK

Recently, several materials were reported on Metal Oxides (MO_x), polymer, and carbon-based composites to fabricate pH and NH_4^+ sensors in an aqueous and gaseous medium[13][14][15][16]. However, the toxicity, non-biocompatibility, and electrochemical instability make them controversial candidates and limit their filed specific applications in soil. In the present work, interdigitated electrode (IDE) modified Graphene -Carbon (G-C)/Zinc Oxide (ZnO) and multiwalled carbon nanotube (MWCNT) /Zinc Oxide (ZnO) active layers were taken separately, tuned in the soil pH and NH_4^+ ions detecting applications respectively.

The ZnO, the traditional n-type (II-VI group) wide bandgap (3.2 eV) semiconductor with hexagonal wurtzite structure, has appeared to be a reasonable preference amongst the MO_x[17][18][19][20]. The ZnO is considered non-toxic, biocompatible, cheaper synthesis technique and abundant availability make them remarkable for sensing applications. It is one of the amphoteric materials and thus can create oriented dipoles or surface bonds by adsorbing (H^+, OH^- and NH_4^+) ions in analyte samples. The traditional glass-based pH sensors are bulky and require reference and counter electrodes such as Ag/AgCl and Pt. Similarly, different methods are used to operate pH and NH_4^+ sensor techniques such as potentiometric, capacitive, chemi-resistive, an ion-sensitive field-effect transistor (ISFET), etc. Screen-printed structures have been used extensively in the pH sensing process. However, the modification resulting in introducing sensitive material or changing the morphology of the printed form, etc.,

makes it cumbersome. Apart from all, the narrow range of detection studied, and the choice of the substrate are some of the other challenges. IDE structures have gained enough attention for various sensing applications in recent trends. The high sensitivity, biocompatibility, lower cost of operation, fast response, and smaller structure are critical requirements for monitoring system design.

3. OBJECTIVES

i. To synthesize G-C/ZnO and MWCNT/ZnO nanocomposites individually via hydrothermal and chemical reflux method and study the chemical composition, structural, morphological characterization of the active materials and electrodes.
ii. To investigate the electrochemical performance of the IDE modified G-C/ZnO active layers for pH sensing applications.
iii. To investigate the electrochemical performance of the IDE modified F-MWCNT/ZnO composite active layers for NH_4^+ ion sensing applications.
iv. To design and integrate the ML-assist soil condition monitoring system using IoT technology.

i. THESIS ORGANIZATION

The thesis is organized into seven chapters, and the general description of each chapter is given as follows.

CHAPTER 1; INTRODUCTION: Describes introduction, which consists of background and motivation of the research, soil definition, soil profile, soil composition, soil classification, soil properties, need for soil pH and NH_4^+ measurement, the scope of the present work with major objective and organization of the thesis.

CHAPTER 2; LITERATURE REVIEW: Discusses the detailed literature review starting with the significance of pH and NH_4^+ content measurement, sensor electrode design and materials, active layer materials used. It also

describes the working mechanism of electrochemical sensors and available electrochemical detection methods for pH and NH_4^+ sensors.

CHAPTER 3; EXPERIMENTAL METHODS: Deals with the fabrication methods and the characterization techniques of the nanomaterials for electrochemical sensing applications used by the researcher. It also describes the detailed specifications of microscopy and electrical characterization tools used to fabricate and characterize the nanomaterials and device.

CHAPTER 4; GRAPHENE-CARBON INK MODIFIED ZINC OXIDE NANOPARTICLES BASED SENSOR FOR SOIL PH MEASUREMENT APPLICATIONS: Discusses the simulation, fabrication, and characterization of the Graphene- Carbon (G-C) modified Zinc Oxide (ZnO) nanoparticles (NPs) based active layer. It also explains Graphene- Carbon (G-C) modified Zinc Oxide (ZnO) nanoparticles based on active layer-based pH sensor fabrication and characterization.

i. Fabrication of screen-printed IDE modified ZnO Nanoparticles based active layer.

Materials and Equipment:

The IDE is developed using graphene-carbon ink (C2171023D1: Graphene Carbon Ink: BG04, Sun Chemical). The Zinc oxide (ZnO) nanoparticles dissolved in ethanol (C2H5OH, MW: 46.07 g/mol, Thermo Scientific) solvent are used for fabricating the active layer for pH sensing. The morphological and structural characteristics of the spin coated ZnO layer are analyzed using scanning electron microscopy and X-ray diffraction. The screen-printed IDE structure is imaged using an optical microscope. The hydrophilicity of the ZnO layer is analyzed using contact angle measurement. Further, the electrical characteristic, i.e., change in impedance response is monitored.

Experiment:

The IDE is developed on a paper substrate using the screen-printing technique. The IDE is printed on the paper substrate in three configurations, i.e., single-layered, double-layered, and triple-layered. The optimized layer configuration is obtained based on their impact on pH sensing properties. 2 wt. % solution of ZnO nanoparticles

dissolved in ethanol solvent is prepared by ultrasonication for 2 hours at room temperature. Later the solution (0.5 mL) drops were cast on all the three different coated layers (single, double, and triple) of IDE structures. The process was repeated 10 times to attain the desired thickness. The coated IDE structure is calcinated at 60 ˚C for 24 hours. Further, the connection points are obtained using wiring followed by dielectric placement to insulate the connection. Later the sensor is utilized for the pH monitoring process.

Result and Discussion:

The surface morphology of the G-C-based IDE and ZnO-NPs based active layer is investigated using scanning electron microscopy (SEM). The G-C ink printed surface, the boundary between the print-ed structure, and the substrate is shown. The darker contrast area is observed as the paper, and the ink structure are observed in the lighter contrast area. Moreover, it also displays the random distribution of carbon and graphene network. On the other hand, the images taken at lower magnification for ZnO modified printed electrode shows distributed spherical particles. The diffractograms of the printed electrode, ZnO nanoparticles, and the modified printed electrode with ZnO are displayed. The printed electrode diffractogram displays a peak of carbon around 27º. However, the broadness in the peak observed is contributed by the presence of graphene nanosheets. While the diffractogram of ZnO (red line) displays the traditional peaks at 31.7º, 34.4º, 36.1º, 47.4º, 56.4º, 66.3º, 68.1º and 69.2º corresponding to (100), (002), (101), (102), (110), (103), (112) and (201) respectively. The results agree with the standard peaks observed for hexagonal wurtzite structure (ICDD card no: 36-1451). The sharp peaks indicate the high crystallinity of the nanoparticles. The peaks observed for the modified printed electrode with ZnO (black line in the inset) show the presence of a combination of both the peaks (Carbon and ZnO).

ii. Evaluation of pH sensing performance

Experiment:

The pH sensing performance of the developed sensor is monitored using the LCR meter through monitoring the change in impedance. The pH samples are prepared to correspond to the target range i.e., pH 2 to pH 9. Electrochemical impedance spectroscopy is carried over the range of 40 Hz to 100 kHz using a 1 Vpp sine wave for the target pH range. The list sweep parameters such as impedance magnitude (R-

X) and double-layer capacitance (Cdl) are extracted in the single trigger computation. All the measurements are carried out at room temperature (30 ± 2 ˚C). Further, to analyze the pH sensing performance of the sensor towards soil pH level. Four different soil samples are prepared (following the standard protocol for the pH measurement) with a pH value of 2, 4, 6, and 8. Initially, the sensor impedance is monitored under the expected ambient conditions followed by the change in impedance magnitude towards prepared soil samples (pH 2-8).

Result and Discussion

The fabricated pH sensor showed a proportional decrease in impedance magnitude with respect to the increase in the frequency level (40 Hz – 10 kHz). Furthermore, the impedance value drastically decreases and holds up with the increase in frequency up to 100 kHz.

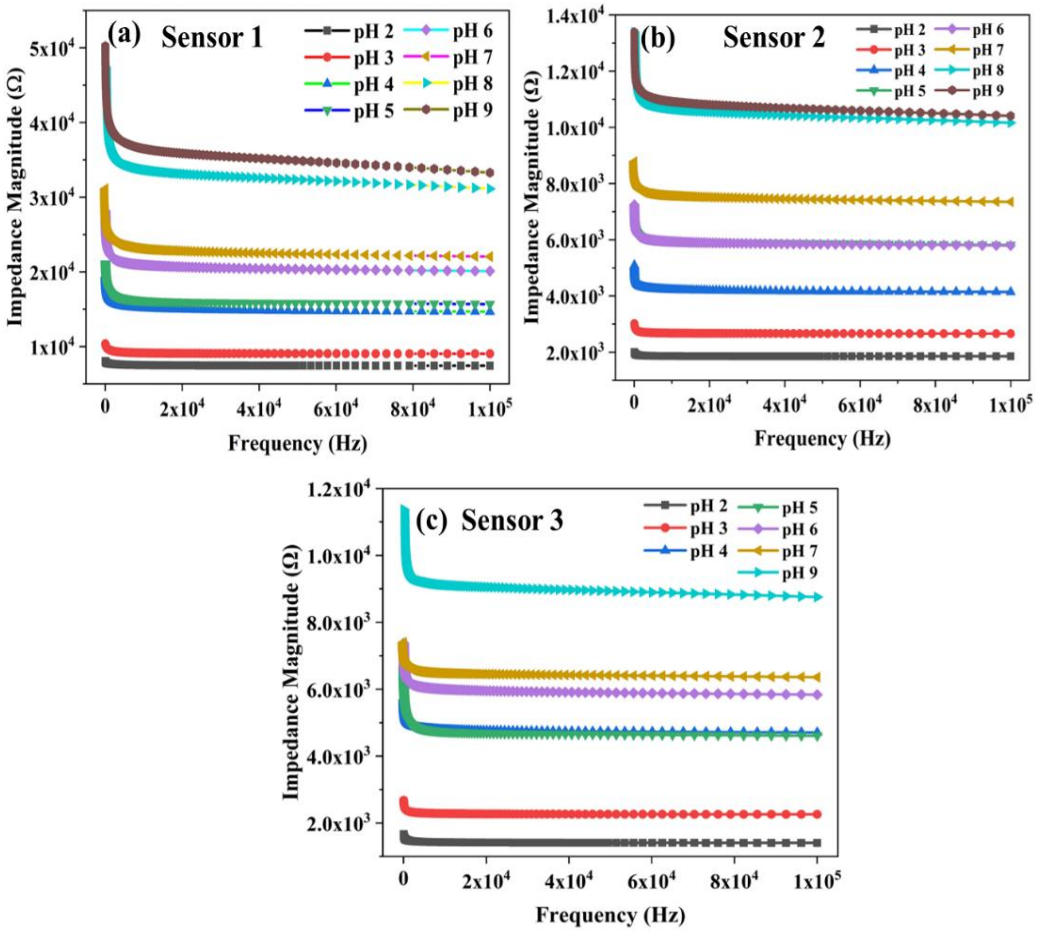

Figure 1 Comparative analysis of pH sensing performance of (a) sensor 1, (b) sensor 2 and (c) sensor 3 from pH 2-9.

A similar pattern was observed for all the three sensor conditions (Figure 1a, b, and c). Even though $|Z_{max}|$ is higher at a lower frequency (40 Hz) level, but stabilized signals are quite unstable and stabilizes only as the frequency level is increased from 40 Hz to 1 kHz, which records the $|Z_{max}|$ value of ~50.2 KΩ. The $|Z_{max}|$ vvalues were comparatively stable for sensor 1 with a maximum variation of ± 2 KΩ. It can be observed that the electrochemical response of the device shows a linear increase of impedance magnitude with an increase in pH levels. The correlation coefficient (R^2) and sensitivity of the fabricated device are calculated in the selective range and recorded in Table 1. Upon close inspection of the responses, the sensor 1 results displayed appreciable sensitivity (6.21-3.99 kΩ/pH), which is about four folds higher than that of sensors 2 and 3. Moreover, the sensitivity and the correlation coefficient (R^2) estimated at 1 kHz is stable and also the highest amongst all the other tabulated values

Table 1 Change in sensitivity and correlation coefficient (R^2) comparison based on pH sensor type and frequency.

Sensor Type	Sensitivity (kΩ/pH)	Adj. R square	Frequency (kHz)
Sensor 1	6.21	0.94685	1
	4.68	0.9461	5
	4.21	0.94808	10
	3.99	0.95153	50
Sensor 2	1.69	0.94457	1
	1.4	0.9545	5
	1.34	0.95806	10
	1.30	0.95984	50
Sensor 3	1.30	0.92961	1
	1.10	0.95305	5
	1.05	0.95487	10
	1.01	0.95365	50

CHAPTER 5; MULTIWALL CARBON NANOTUBE MODIFIED ZINC OXIDE ACTIVE LAYER-BASED SENSOR FOR SOIL AMMONIUM MEASUREMENT APPLICATIONS:

Discusses the fabrication, and characterization of the multi-wall carbon nanotube (MWCNT) modified Zinc Oxide (ZnO) nanoflowers (NFs) active materials. It also describes multi-wall carbon nanotube (MWCNT) modified Zinc Oxide (ZnO) nanoflowers (NFs) based Ammonium (NH_4^+) sensor fabrication and characterization.

i. Fabrication of screen-printed IDE modified F-MWCNT/ZnO-NFs based active layer.

Materials and Equipment:

Multi-wall carbon nanotube (MWCNT), Zinc nitrate hexahydrate ($H_{12}N_2O_{12}Zn$), Sodium hydroxide (NaOH), Hexamine($(CH_2)_6N_4$), Copper (Cu), Fiber epoxy resins, Dimethyl sulfoxide (DMSO), Nitric acid (HNO_3), Ammonium hydroxide (NH_4^+OH) and Ethanol are the precursor materials and solvents used to formulate the F-MWCNT/ZnO-NFs nanocomposites. The precursor materials and analytes were purchased from Sigma Aldrich. The surface orientation of the F-MWCNT/ZnO-NFs structures was studied using field emission scanning electron microscopy (FESEM) with energy-dispersive X-ray spectroscopy (EDS). Crystal phase and orientation of F-MWCNT, ZnO, and F-MWCNT/ZnO nanocomposites were examined using an X-ray diffractometer (XRD). Further, the electrochemical performance of the NH_4^+ detection device was measured using an Agilent 4294A precision impedance analyzer system. Measurements were repeated and analyzed using multiple sets of sensors.

Experiments:

F- MWCNT was functionalized using ZnO nanoparticles to form F-MWCNT/ZnO-NFs nanoflowers (NFs) structures. MWCNT is added with Nitric acid (HNO_3) in the ratio of 1:1.5 solution is made homogeneous. The obtained solution is further refluxed for 8 hours at 110°C, consequently, F-MWCNT powder is treated with 0.1, 0.3, and 0.5 M Zn $(NO_3).6H_2O$ to get the ZnO in the proportion of 1%, 3%, and 5%. Three variants of nanocomposites were synthesized by varying the MWCNT: ZnO ratio.

The binding agent (0.01 M Hexamine) is added to the respective homogeneous nanocomposite solutions to create three types of sensors (S1, S2, and S3) with varying ZnO: MWCNT ratios. The mixture was refluxed for 3 hours at 120°C and the precipitate was dried at 80°C for 10 hours to get the F-MWCNT/ZnO-NFs composites. The synthesized products were investigated in terms of morphological and structural properties. The prepared F-MWCNT/ZnO nanocomposites are dispersed in the solvent dimethyl sulfoxide ($(CH_3)_2SO$). Further, the dispersed solution was deposited on the IDE using a temperature-controlled spin coating unit at the rate of 3000 RPM for 20 seconds with a three-step programming process. The same deposition process was repeated twice to obtain a thick uniform pattern of the IDE surface's F-MWCNT/ZnO active layer.

Results and Discussion:

The potential of the electrode and active materials for electrochemical sensor application could be evaluated by nanocomposites' size and surface morphology. Evident from the FESEM studies on MWCNT, F-MWCNT, F-MWCNT/ ZnO-NFs composites with the proportion of 1:1, 1:3, and 1:5 the morphology of F-MWCNT/ZnO-NFs composites with varying ZnO percentages were distinctly different. Formation of NFs inclusions over the F-MWCNT was observed. The majority of the MWCNT and F-MWCNT are uniformly distributed in high compactness with almost parallel alignment to the surface. ZnO NFs are assembled in bunches that contain sub-NFs. Further characterization of the NFs attributed a hexagonal structure to NFs, confirming good crystallinity. We noticed that the ZnO percentage in the composite defines the orientation of the NFs so that their branching and petal size is proportional to the ratio of ZnO (1 to 5%).

The XRD results of F-MWCNT have shown the strong peaks at diffraction angle 2θ = 22.46° and 25.31° and corresponded to the plane of the MWCNTs phase as stated in the JCPDS card No.41-1487[21]. The observed crystalline peaks of the ZnO are perfectly indexed and well-matched with the standard data (JCPDS card No.35-1451). The ZnO consists of a strong diffraction peak at the (002) plane and its location at angle 2θ = 35.43°. So, we can confirm that ZnO nanostructures have a hexagonal wurtzite morphology with a high c-axis. No other peak related to impurities was detected in the spectrum, which further confirms the synthesized materials were of high purity and matches well with the standard crystallographic data (ZnO: JCPDS

01-076-0704, C: JCPDS No. 00-026-1080). The strong diffraction peak at the angle 2θ of 25.58° can be indexed as the C (002) reflection of the hexagonal graphite structure and corresponding to the MWCNT, which confirms the formation of composites and completely reduced its peaks in the F-MWCNT/ZnO-NFs nanocomposites because of ZnO-NFs embedded on the entire surface of F-MWCNT. As a function of the ZnO concentration ratio, peak intensities of F-MWCNT and ZnO varies within nanocomposite samples (1:1, 1:3, and 1:5). It i evidence that increasing the concentration of ZnO will decrease the peak intensity of the F-MWCNTs and ZnO peaks are becoming more intense. The peaks intensity of F-MWCNT/ZnO-NFs nanocomposites (1:1, 1:3, and 1:5) decreased compared with the untainted ZnO peaks. This indicates that the crystallinity of the materials decreases on composite formation. The average crystallite size was calculated from the diffraction peaks using the Scherer formula for F-MWCNT, ZnO and MWCNT/ZnO nanocomposites were found to be 2.193 nm 39.42 nm and 21.15 nm respectively.

ii) Evaluation of NH_4^+ sensing performance

Experiment:

The NH_4^+ sensing performance of the developed device is monitored using the Agilent 4294A precision impedance analyzer system through monitoring the change in impedance. Laterite soil samples were obtained from the Joint Director Agriculture Office, Dakshina Kannada District, Karnataka, India. The arbitrary variation of soil pH, electrical conductivity (EC), organic Carbon (O.C) and available NPK content affects the fertigation process and thus crop yield[22]. The pH 7 carried laterite dry soil named sample 1 was added to the standard NH_4^+ solution and samples were prepared to correspond to the target range i.e., 0.1-100 mM. Further, contact pads of the device were connected to the probe station using an impedance/gain phase analysing system. The electrochemical performance of the device is carried over the range of 40-100 kHz using a 1 Vpp for the target NH_4^+ range. The list sweep parameters such as impedance magnitude (R-X) and double-layer capacitance (C_{dl}) are extracted in the single trigger computation. All the measurements are carried out at room temperature (30 ± 2 ˚C). Initially, the impedance of the sensor is monitored under the normal ambient conditions followed by monitoring the change in impedance magnitude towards prepared soil samples (0.1-100 mM).

Results and Discussion:

The Figure 2 shows the impedimetric performance of the NH_4^+ sensor 3 across continuous frequency sweep (40 Hz – 100 kHz) in pH adjusted (pH 4, pH 7 and pH 9) NH_4^+ analyte solutions.

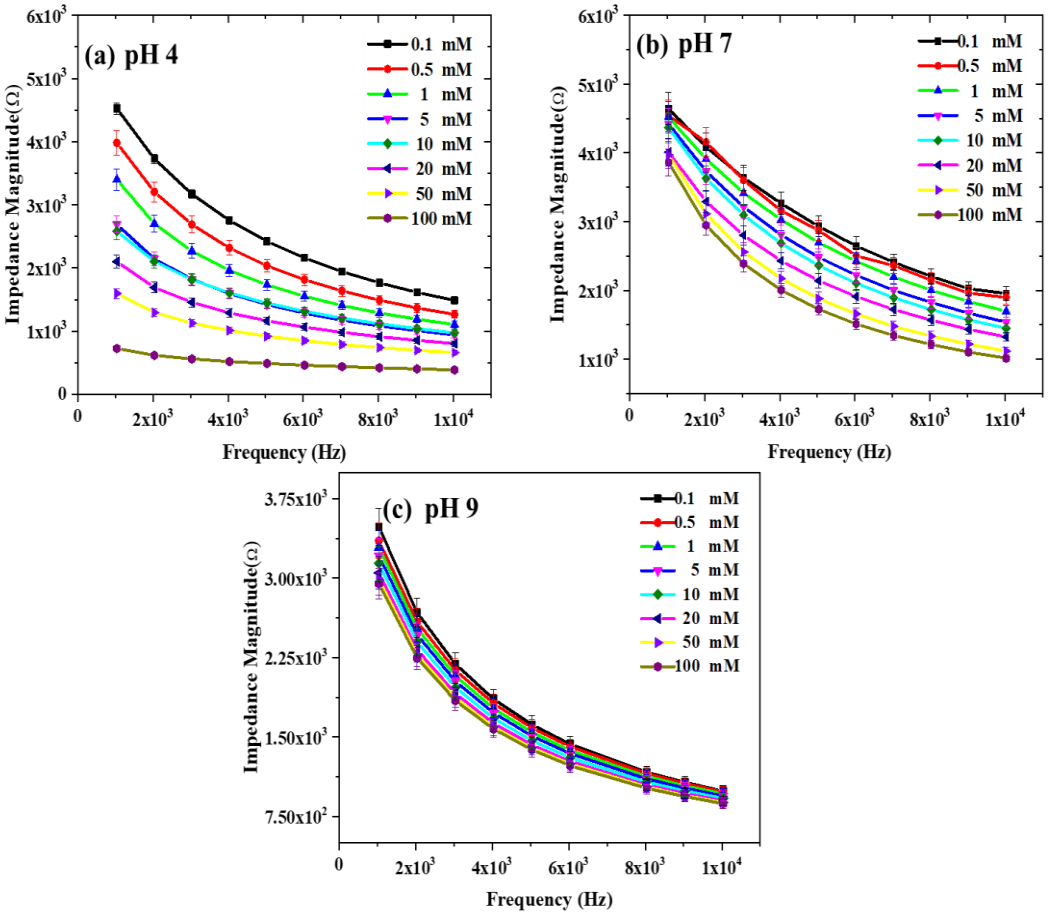

Figure 2. Impedance magnitude (Ω) versus frequency response of the sensor 3 in the (a) acid, (b) neutral, and (c) alkaline sample conditions.

A proportional decrease in impedance magnitude was observed with respect to the increase in the frequency level (40 – 10 kHz). Furthermore, with the increase in frequency up to 100 kHz, the impedance value drastically decreases and holds up. Results indicate that higher pH conditions cause an enhanced impedance value for sensor 3. It can be noted that impedance values of the sensor decreased with increasing NH_4^+ levels in acid (Figure 2a), neutral (Figure 2b) and alkaline ((Figure 2c) conditions. The device sensitivity to NH_4^+ was also found to vary with pH conditions. Critical values such as the $|Z_{max}|$ and the frequency dependency of $|Z|$ were found to vary from device to device. $|Z_{max}|$ values for sensor 3 operated at pH 4

was ~ 10.5% higher when operated in pH 9. The rate of change of $|Z_{max}|$ is highest for pH 4 whereas an increase in Z_{max} was very gradual at pH 7 and 9. On the other hand, the function of NH_4^+ reflected the change in ions concentration in the dielectric medium and causes a change in the sensor impedance magnitude allied with the protonation and deprotonation of the analytes. In addition to that, the sensitivity of the sensors in various pH analyte conditions (pH 4, pH 7, and pH 9) is estimated from the characteristics curve of average impedance magnitude *vs* pH (Figure 5-9).

It can be observed that the electrochemical response of the device shows a linear decrease of impedance magnitude with an increase of the NH_4^+ levels. The correlation coefficient (R^2) and sensitivity of the fabricated device are calculated in the selective range and recorded in Table 2. Upon close inspection of the responses, the sensor 3 results displayed appreciable sensitivity (76.09 ±3.80 Ω/mM), which is about three folds higher than that of neutral conditions (26.18 ±1.30*)* and six folds higher than that of alkaline conditions (12.16 ± 0.60). Moreover, the sensitivity and the correlation coefficient (R^2) estimated at 1 kHz in lower analyte pH condition is stable and also the highest amongst all the other tabulated values. Accordingly, the sensor 3 (pH 4 analyte condition) with an applied frequency condition of 1 kHz is judged as the most sensitive and stable device for NH_4^+ sensing in the desired NH_4^+ range (20 mM).

Table 2 Fabricated NH_4^+ sensor 3 response for selective range about 1-20 mM with acid, neutral and alkaline sample conditions.

NH_4^+ Sensor	**NH_4^+ sample conditions**	**Correlation coefficient (R^2)**	**Sensitivity (Ω/mM)**
Sensor 3	Acid (pH=4)	0.98399	76.09 ±3.80
	Neutral (pH=7)	0.95135	26.18 ±1.30
	Alkaline (pH=9)	0.94865	12.16 ±0.60

CHAPTER 6; MACHINE LEARNING ASSISTED SOIL CONDITION MONITORING SYSTEM USING IOT TECHNOLOGY: Discusses the predictive features for the machine learning model. The most dominant predictors

were identified using feature importance analysis. It also explains the calibration process of soil pH and NH_4^+ sensors and wireless sensor data communication process through the IoT platform.

i. Machine learning based target prediction

Experiments:

Predictors of the model were extracted from the impedance spectra, sample features, and experimental settings (Figure 3 a). Both impedance magnitude and frequency features are used as predictors to capture the dynamics of the original spectra. Individual features were expanded into multiple predictors in order to better represent a non-linear input-output relationship thereby eliminating outliers and reducing computational time[23]. The frequencies at which a fixed change in impedance occurs are taken as the derivative frequency values (f_n) of a spectrum (Figure 3 b). Predictors $f_{0.1}$ to $f_{0.9}$ are the frequencies at which the impedance values are 0.1-0.9 times of Z_{max} from the impedance spectra, we extracted derivative frequencies f_n at $Z_n = n * Z_{max}$ $\{ 0.1 \leq n \leq 0.9\}$.

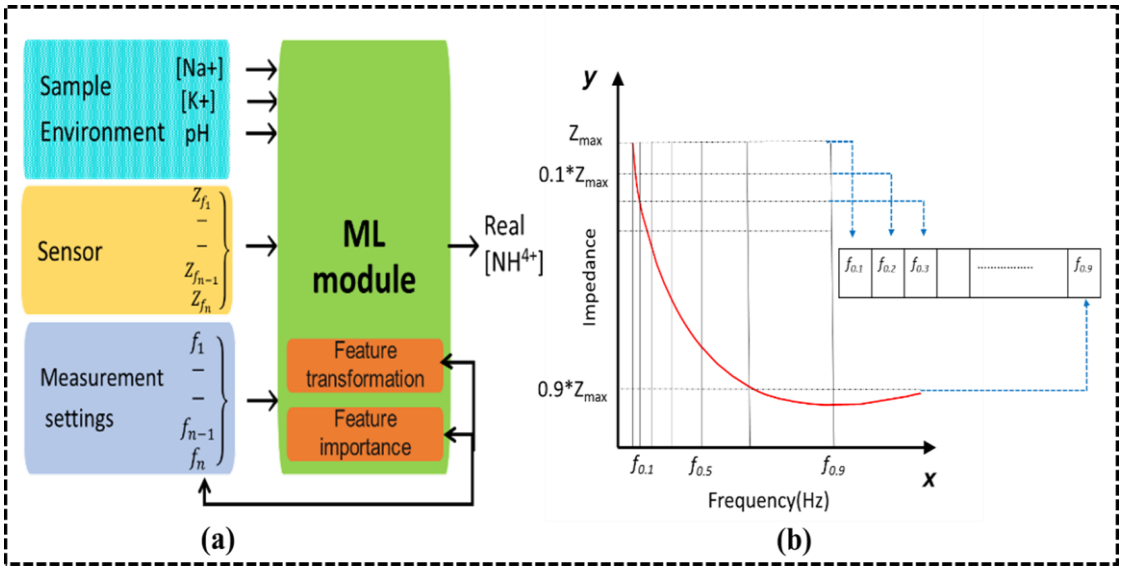

Figure 3 Predictors of the ML model are extracted from Impedance Spectral features, sample parameters, and experimental settings. (b) Predictors $f_{0.1}$ to $f_{0.9}$ are the frequencies at which the impedance values are 0.1-0.9 times of Z_{max} .

We hypothesize that representing the impedance variations as f_n will reduce the dependency of the spectrum on electrode area. f_n starts to increase at the onset of depletion and a maximum value of f_n is observed at $0.9 * Z_{max}$. Although Z_{max}value

is a function of the area of the electrode, the frequency response is influenced by the dielectric property of the material and the environment. The total surface area of an electrode may decrease after cycles of repeated measurements as the nanocomposite structures in the active layer tend to deteriorate. We transformed the impedance features into admittance values in order to improve the model. Raw impedance data were pre-processed using a running mean prior to modelling. But excess data smoothing showed a tendency to eliminate important nonlinear patterns. Hence, we adopted a Box-Cox transformation method that uses separate estimation procedures to transform the impedance (Z) data so that it closely resembles a normal distribution. A Box-Cox transformation was used to estimate the transformation.

$$x^* = \begin{cases} \dfrac{x^\lambda - 1}{\lambda\, x^{\lambda-1}}, & \lambda \neq 0 \\ \tilde{x}\, \log x, & \lambda = 0 \end{cases}$$

The Box-Cox procedure, originally intended as a transformation of a model's outcome, uses maximum likelihood estimation to estimate a transformation parameter λ in the equation which is estimated from the data. Values of λ map to transformations. When λ=1 (no transformation), λ=0 (log), λ=0.5 (square root), and λ=−1 (inverse). For impedance (Z) values, λ was estimated to be -1 which is effectively the inverse transformation. Hence, we adopted the admittance representation in our datasets using the feature constructor tool in Orange. Prediction of target variable concentration (NH_4^+) was done using 28 predictors in which 8 are experimental features and 20 are impedance and frequency features of the Frequency-impedance (F-Z) spectrum. The S1, S2 and S3 are categorical predictors that indicate the type of sensor. The extracted features of the spectra are stored in a structure with a sensor and session ID number encoded in CSV (Comma-Separated Values) file for each impedance spectrum. Missing values were replaced with the median value of the predictor. 80% of dataset is assigned as training data set and the other 20% were assigned for testing. The accuracy of the ML regression models was analyzed using a confusion matrix to compare the predicted and true values.

Result and Discussion:

From the confusion matrices, scoring frameworks such as CA (Accuracy classification score), Precision (precision computation), recall (computation of true positives and false negatives), F1 score (weighted average of precision and recall) and

AUC (stored predictions and actual data in model testing) were obtained to evaluate the prediction efficiency of each model. Scoring framework takes the decimal values of probability between 0 and 1. Evident from the Confusion matrices are the prediction accuracy of all the models among which RF (Random Forest) is the most accurate. Among all the models that we tested, RF model was the most efficiency in predicting the concentration range, which has a precision score of 0.83-0.89 depending upon the predictor variables. Using impedance only dataset, RF displayed a precision of ~0.83. Precision values of the RF model increased from 0.83 to 0.85 when transformed 1/Z values were used. The precision of the RF model was increased further to ~0.87 after including derivative frequency (f_n) predictors. Accuracy was highest for the RF model when admittance (1/Z) was used as a predictor instead of impedance values. The prediction accuracy of the model was lower for samples in low pH solutions. This may be attributed to high variance in Z values in low pH solutions. All other models like ANN and kNN had lower prediction accuracy (<0.70). SVM models with four different kernels (polynomial, sigmoidal, linear, and radial basis function) were analyzed. However, SVM showed the least accuracy (0.24-0.47) while testing for unknown samples. Extraneous predictors erode the performance of a model and also increases computational cost. It is important to identify a subset of predictors with high prevalence. Among the predictors, some of them have a significant influence on the response of the model. Feature importance was tested by permuting the predictors and measuring the decrease in accuracy. The IG scores of various predictors are ranked based on highest and lowest precedence features. We evaluated the information gain for each variable in order to select only those variables that maximizes the information gain. IG score provides a baseline for comparison; some of the features are removed based on feature importance scores. Among three datasets analyzed, each consisting of ~150 data points and 18 features, Z_{2k}, the Z value corresponding to the impedance at 2 kHz, had the highest IG score 0.544 which is higher among all Z predictors (Z_{1k-10k}). IG scores were higher for f_n predictors. Among them $f_{0.8}$ had the highest score (0.574). S predictors, S1, S2, S3, was found to have low info gains (~0.047). Following points summarizes our findings from the feature analysis.

- It was clear from the IG scores that categorical S-predictor parameter S3 has a higher significance than S2 and S1

- Impedance predictors had higher IG scores than Admittance.
- Frequency predictors (f_n) had a higher significance than impedance or Admittance predictors. Among the f_n predictors, $f_{0.8}$ (0.574) had the highest significance and $f_{0.9}$ (0.43) had lowest significance.
- The effect of interfering ions and pH were consistent across all types of devices (S1, S2 and S3). For all datasets, IG scores for pH was 0.33 and interfering ion concentrations scores were 0.157.

ii. Design and prototype of IoT enabled soil condition monitoring system.

Hardware:

NodeMCU development kit, G-C modified ZnO based pH sensor, MWCNT modified ZnO based NH_4^+ sensor and computer and 3D printed sensor package hardware were used.

Software:

ThingSpeak IoT platform, application programming interface (API) software and Arduino integrated development environment (IDE) were used.

Experiment:

The researcher developed real time pH and NH_4^+ level monitoring system, which is facilitated using Node MCU microcontroller platform (ESP8266). The wireless monitoring system comprises of fabricated sensors, signal processing unit, Wi-Fi module and DC power supply unit. The system was powered by a 3V DC supply unit and a 32-bit microcontroller combined with ESP-12 module (Wi-Fi SoC). In the signal conditioning circuit, a $10\ k\Omega$ resistor and 1 kHz frequency generator circuits were connected in series with the sensors to get voltage signal as an input for the NodeMCU development kit. The system design parameters include the repeatability and stability data of the change in impedance measurements of the calibrated pH and NH_4^+ sensor to predict the corresponding pH and NH_4^+ level in an aqueous and soil environment.

Results and Discussion:

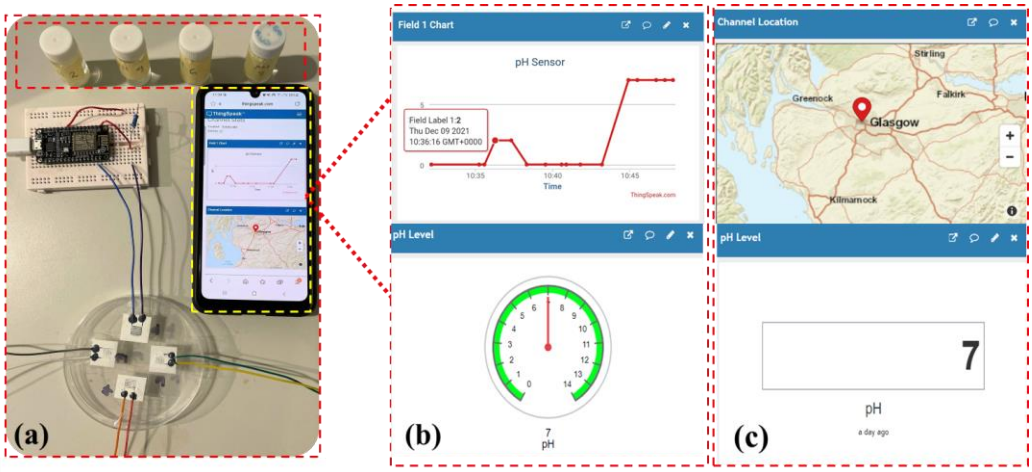

Figure 4 (a) IoT enabled pH monitoring system; (b) Data displayed in the application showing the change in the values at multiple cycles (c) Data displaying the geographical location of the measurement spot.

The ThingSpeak analytics platform is used to visualize the live data streams in web applications. As depicted in Figure 4 a, the detected pH data is received and displayed in real-time on a smart device. Figure 4 b is the front-end visualization system, representing both previously recorded and real time pH measurements. While Figure 4 c illustrates the geographical information (University of Glasgow) of the measurement spot of the pH sensor along with an effortless display highlighting the pH level.

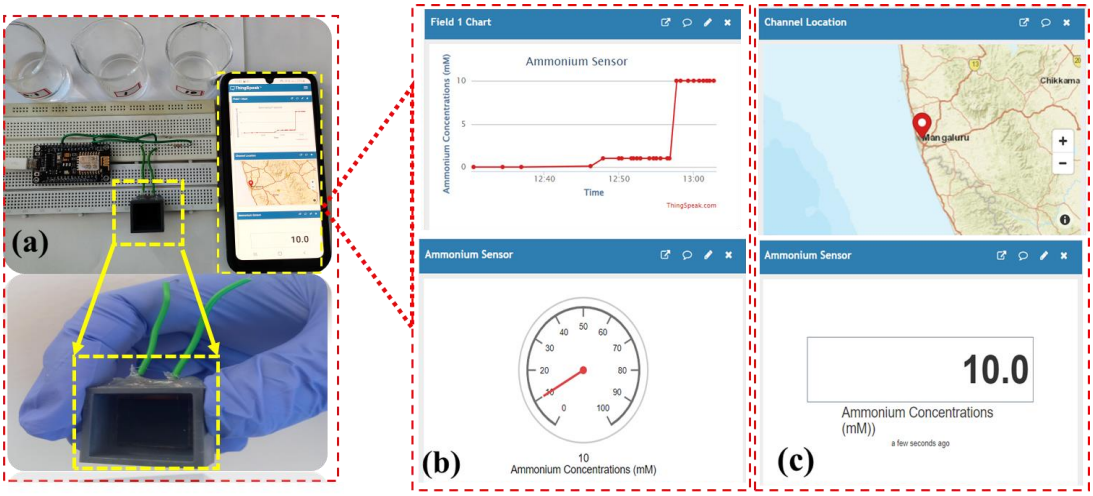

Figure 5 (a) IoT enabled NH_4^+monitoring system; (b) Data displayed in the application showing the change in the values at multiple cycles (c) Data displaying the geographical location of the measurement spot.

As depicted in Figure 5 a, the detected NH4+ data is received and displayed on a smart device in real time. Figure 5 b is the front-end visualization system, representing both previously recorded and the real-time NH_4^+ measurements. Figure 5 c illustrates the geographical information (Mangalore University) of the measurement spot of the NH_4^+ sensor along with an easy display highlighting the pH levels.

CHAPTER 7; CONCLUSIONS AND FUTURE SCOPES OF THE WORK: Shows the conclusion of the thesis and recommendations for future outlooks of the works.

The researcher presents the design and development of soil pH and NH_4^+ detection systems using nanomaterials-based sensors starting from materials synthesis to system development. The report explains nanocomposite active material synthesis, electrode design, characterization, sensor fabrication, calibration, and system development and testing using internet of things (IoT) technology as wireless data communication means. The ZnO was selected as a biocompatible active material for the electrochemical pH and NH_4^+ sensor. The surface morphology, chemical compositions, and crystalline structure as-synthesized ZnO and MWCNT/ZnO nanocomposites were studied using FESEM, EDAX, and XRD, respectively. Similarly, the electrochemical performance of the developed sensors was studied by using an electrochemical impedance analyzer. To enhance the impedance performance of the developed sensor system, interdigitated electrodes (IDE) were incorporated, where electrical signals are generated and instantly transmitted to the processing systems. The electrode geometry, such as electrode width, interspace, length, and several electrodes, are optimized to get the enhanced target signal from the sensor.

The screen-printed pH and NH_4^+ sensors are fabricated using the impedimetric method. The pH sensor was fabricated using screen-printed Graphene- Carbon IDE modified ZnO nanoparticle-based active layer. The nanostructured active layer provides large surface areas and binding sites for the target H^+ and OH^- ions. At the same time, biocompatible and disposable paper-based sensor platforms allow ease in operation for soil pH monitoring. The fabricated sensor shows nearly three orders of change in impedance magnitude in the pH range of 2 – 9. Moreover, it exhibits a high sensitivity of 5.01 kΩ /pH (2-8) with a correlation coefficient (R^2) of 0.93 and displays high stability in the response. Further, the NH_4^+ sensor was fabricated using a

screen-printed IDE modified F-MWCNT/ZnO-NFs composite based active layer. The F-MWCNT/ZnO-NFs composite active layer provides large surface areas and binding sites for the NH_4^+ target ions. In contrast, biocompatible sensor active layers allow ease in operation for soil NH_4^+ monitoring. The fabricated sensor exhibits a sensitivity of 76.09 ±3.80 Ω /mM (1-20) with a correlation coefficient (R^2) of 0.98. The essential parameter of the sensor signal was unaffected by the presence of interfering cations and displayed high stability in the response. The pH and NH_4^+ sensor are energy efficient, fabricated in a simple and economical screen-printing method, requires low power for sensor operation, and the target signal is highly stable. In addition, the Machine Learning (ML) based decision support tool, the new frame of reference has been designed to interpret the features of impedance spectra and predict the real analyte concentrations by mitigating the effects of non-linearity and impedance drifts. ML analysis has led to the identification of dominant predictors of our sensing system. The result confirmed the possibility of integrating a custom ML module in an impedance sensing system to mitigate the detrimental effect of interference ions and pH on the sensitivity and selectivity of the sensor. Different models such as K-Nearest Neighbor, Random Forest, Neural Network, Naive Bayes, and Logistic Regression support have been contrasted and discussed.

The wireless data communication also explores more avenues towards independent usage and field-specific monitoring web applications. The embedded system development comprises both hardware and software parts. The hardware components are NodeMCU development kit, pH, and NH_4^+ sensors, while the software components are Arduino IDE, ThingSpeak application program, and API. The system monitors the soil pH and NH_4^+ level through the web application via a personal channel made by the consumer at a distance. This can significantly contribute towards sustainable smart agriculture practices. Finally, the researcher can conclude that this work is unique because it is the first that involves nanomaterials based biocompatible-assisted sensor system for this particular application.

A list of references, and notable outcomes of the research work was also included in the final part of the thesis report.

NOTABLE OUTCOMES OF THE RESEARCH WORK

A. List of Journal Papers Published:

1. Machine learning-assisted Ammonium Detection Using Zinc Oxide/Multi-Walled Carbon Nanotube Composite based Impedance sensors, *Sci.Rep*. 11, 24321 (2021).
   Akshaya Kumar A, Naveen Kumar S K, Pradeep Marimuthu, Aiswarya Baburaj, Michael Adetunji, Terrance Frederick, Renny Edwin Fernandez
   https://doi.org/10.1038/s41598-021-03674-1.

2. Real-Time Sensing of Soil Potassium Levels Using Zinc Oxide-Multiwall Carbon Nanotube-Based Sensors, IEEE Trans Nanobioscience, 20 (1), 50-56 (2021).
   Akshaya Kumar A, Naveen Kumar SK, and RE Fernandez
   https://doi.org/10.1109/TNB.2020.3027863.

3. Hydrothermal Growth of Zinc Oxide (ZnO) Nanorods (NRs) on Screen Printed IDEs for pH Measurement Application, Journal of The Electrochemical Society (JES) 166 (9), B3264-B3274 (2019).
   Akshaya Kumar A, Naveen Kumar SK, Almaw Ayele Aniley, RE Fernandez, S Bhansali
   https://doi.org/10.1149/2.0431909jes

4. Comprehensive Review on pH and Nutrients Detection Sensitive Materials and Methods for Agriculture Applications, SENSOR LETTERS, (17), 1–8, (2019).
   Akshaya Kumar A and Naveen Kumar SK
   https://doi.org/10.1166/sl.2019.4126.

5. Fabrication of interdigitated electrodes (IDEs) modified with sensitive layers of ZnO nanorods and nanoflowers, AIP Proceedings, 2162(020076),1-6 (2019).
   Akshaya Kumar A and Naveen Kumar S. K
   https://doi.org/10.1063/1.5130286.

6. Integration of interdigitated electrodes (IDEs) with ZnO nanoflakes (Nfs) active layers, AIP Proceedings, 2244 (1),1-5 (2020).
   Akshaya Kumar A and Naveen Kumar S. K
   https://doi.org/10.1063/5.0009499.

7. Hydrothermal Growth of Zinc Oxide (ZnO) Nanorods (NRs), Structural, and Chemical Composition Studies for pH Measurement Sensor Applications, ECS Transactions, 88 (1) 437-447 (2019)
   Naveen Kumar S K, **Akshaya Kumar A**, Almaw Ayele Aniley, S Bhansali, RE Fernandez
   https://doi.org/10.1149/08801.0437ecst.

8. Thin Film Dual Probe Heat Pulse (DPHP) Micro Heater Network for Soil Moisture Content Estimation in Smart Agriculture, Journal of The Electrochemical Society (JES) 166 (2), B63-B6(2019).
   Almaw Ayele Aniley, Naveen Kumar SK, **Akshaya Kumar A**, RE Fernandez, S Bhansali
   https://doi.org/10.1149/2.0511902jes

9. Fabrication, Characterization, and Comparison of Nanocrystalline NiMn2O4 and NiZn02MnO4 NTCR Ceramic Thermistor Powders, Journal of Nanoscience and Technology 5 (1), 603–606 (2019).
   Almaw Ayele Aniley, S.K. Naveen Kumar S K and **Akshaya Kumar A**
   https://doi.org/10.30799/jnst.201.19050106

10. Nanoceramic NiMn2O4 Powder-Based Resistance Thermometer for Soil Temperature Measurement Application in Agriculture, ECS Transactions 88 (1), 455-470(2019).
    Naveen Kumar S.K, Almaw Ayele Aniley, **Akshaya Kumar A**, RE Fernandez, S Bhansali
    https://doi.org/10.1149/08801.0455ecst

B. List of Book Chapters Published:

1. Fabrication of Interdigitated Electrodes (IDEs) by Screen Printing Technology and Their structural Studies, Nanostructured Smart Materials, vol (1) p.p. 11, eBook ISBN9781003130468, Apple Academic Press, Taylor & Francis Group (2021).
   A. Akshaya Kumar, S. K. Naveen Kumar, Almaw Ayele Aniley
   https://doi.org/10.1201/9781003130468.

2. Dual Probe Heat Pulse (DPHP) Method Soil Moisture Sensor, Using Advanced Materials-Based Thermistor and Fluorine Doped Tin Oxide (FTO) Thin Film Electric

Heater, Nanostructured Smart Materials, vol (1) p.p. 11, eBook ISBN9781003130468, Apple Academic Press, Taylor & Francis Group (2021). Almaw Ayele Aniley, S. K. Naveen Kumar, and **A. Akshaya Kumar**, https://doi.org/10.1201/9781003130468.

3. Indium Doped Tin Oxide (ITO) Nano Powder-Based Electric Heater Fabrication and Characterization, Nanostructured Smart Materials, vol (1) p.p. 11, eBook ISBN9781003130468, Apple Academic Press, Taylor & Francis Group (2021). Almaw Ayele Aniley, S. K. Naveen Kumar, and **A. Akshaya Kumar** https://doi.org/10.1201/9781003130468

C. List of Papers Presented in Conference:

1. Smart Impedance Sensing for Metal Oxide-Carbon Nanotube Nanocomposites, ECS 2021 *Meet. Abstr*. **MA2021-02** 1931.
   Akshaya Kumar A, Naveen Kumar S K, Pradeep Marimuthu, Aiswarya Baburaj, Michael Adetunji, Terrance Frederick, Renny Edwin Fernandez.
   https://doi.org/10.1149/MA2021-02571931mtgabs

2. F- MWCNT/ ZnO Nanocomposites for Real-Time Detection of Ammonium Level in Paddy Field, ECS 2021 *Meet. Abstr* IMCS 01-1330.
   Akshaya Kumar A, Naveen Kumar SK, Aiswarya Baburaj, RE Fernandez and Ajit Khosla
   https://doi.org/10.1149/MA2021-01541330mtgabs
3. ZnO Nanorods Based Miniature Sensor Networks for Continuous Monitoring of Soil pH in Smart Agriculture, *Meet. Abstr*. MA2020-01 2217, Canada,
   Akshaya Kumar A, Naveen Kumar SK, Shekhar Bhansali, and Ajit Khosla
   https://doi.org/10.1149/MA2020-01292217mtgabs.
4. Assimilation of Interdigitated Electrodes (IDEs) with ZnO Nanorods (NRs) for Potassium Measurement Application, ECS 2020 *Meet. Abstr*. MA2020-01 2218, Canada.
   Naveen Kumar SK, **Akshaya Kumar A**, Shekhar Bhansali, and Ajit Khosla
   https://doi.org/10.1149/MA2020-01292218mtgabs
5. Development of Cu/F-MWCNT/ZnO Based Active Layer for Long Term Soil Urea Measurements, **Akshaya Kumar A**, Naveen Kumar SK, Aiswarya Baburaj, RE Fernandez and Ajit Khosla, ECS 2021 *Meet. Abstr* IMCS 01-1329 (Digital Meeting)

6. Integration of Interdigitated Electrodes (IDEs) with ZnO Nanoflakes (Nfs) Active Layers, **Akshaya Kumar A** and Naveen Kumar S K, ICPN 2019, Mangalore, Karnataka.
7. Fabrication of Interdigitated Electrodes (IDEs) Modified with Sensitive Layers of ZnO Nanorods and Nanoflowers, **Akshaya Kumar A** and Naveen Kumar S K, ICAM 2019, Kannur, Kerala.
8. Screen Printed IDEs Modified with Zinc Oxide (ZnO) Nanorods (NRs) for Electrochemical pH Sensor, **Akshaya Kumar A,** and Naveen Kumar S K, Young Scientist conference as a part of India International Science Festival (IISF), 2019, Kolkata, India.
9. Fabrication of Interdigitated Electrodes (IDEs) by Screen Printing Technology and their Structural Studies**. Akshaya Kumar A**, Naveen Kumar S.K, Almaw Ayele Aniley and Shekhar Bhansali. ICN 2018, Kottayam, Kerala.
10. Hydrothermal Growth of Zinc Oxide (ZnO) Nanorods (NRs), Structural, and Chemical Composition Studies for pH Measurement Sensor Applications, Naveen Kumar S K, **Akshaya Kumar A**, RE Fernandez, S Bhansali, 4DMS-2018, 26 August 2018 to 30 August 2018, YAMAGATA University, Yonezawa Japan.
11. Fabrication of Interdigitated Electrodes (IDEs) with a nanostructured sensitive layer for electrochemical sensor applications**. Akshaya Kumar A** and Naveen Kumar S K. ICMS-2018, 11 and 12 December 2018, Chennai, Tamilnadu.
12. Structural and optical properties of zinc oxide nanoflowers synthesized using the sol-gel method. **A Akshaya Kumar**, S K Naveen Kumar, Almaw Ayele Aniley, NCASMDT 2018 February 12-13, 2018, Bangalore.

D. List of Papers Communicated to the Journal:

1. Impedance Sensor for Real-Time Ammonium Detection based on MWCNT/ZnO Nanocomposites, **IEEE Trans Nanobioscience**, TNB-00145-2021 (**Revision Submitted**). Naveen Kumar S K**, Akshaya Kumar A**, Aiswarya Baburaj, Michael Adetunji, Renny Edwin Fernandez.

2. Disposable pH sensor on paper using screen-printed graphene-carbon ink modified zinc oxide nanoparticles. **Sensors & Actuators B**, 2022 (**Manuscript Submitted**). **Akshaya Kumar A**, Priyanka Ganguly, Ajay beniwal, Naveen Kumar S K, Ravinder Dahiya.

4. References

[1] World Bank, “Agriculture for Development,” 2008. doi: 10.1596/978-0-8213-7233-3.

[2] D. Cervantes-Godoy et al., The future of food and agriculture: trends and challenges, vol. 4, no. 4. 2014.

[3] S. S. Dr. G. N. Rameshaiah1, JPallavi2 and 1Associate, “Nano Fertilizers and Nano Sensors – an Attempt for,” vol. 3, no. 1, pp. 314–320, 2015.

[4] J. B. Jones Jr., “Plant Nutrition and Soil Fertility Manual,” Plant Nutr. Soil Fertil. Man., no. 2, 2012, doi: 10.1201/b11577.

[5] J. Zhao, Y. Dong, X. Xie, X. Li, X. Zhang, and X. Shen, “Effect of annual variation in soil pH on available soil nutrients in pear orchards,” Acta Ecol. Sin., vol. 31, no. 4, pp. 212–216, 2011, doi: 10.1016/j.chnaes.2011.04.001.

[6] D. Neina, “The Role of Soil pH in Plant Nutrition and Soil Remediation,” Appl. Environ. Soil Sci., vol. 2019, no. 3, 2019, doi: 10.1155/2019/5794869.

[7] F. G. Fernández and R. G. Hoeft, “Illinois Agronomy Handbook Estimating Nutrient Availability Soil Analysis,” pp. 91–112.

[8] Y.-H. Liao and J.-C. Chou, “Fabrication and Characterization of a Ruthenium Nitride Membrane for Electrochemical pH Sensors,” Sensors, vol. 9, no. 4, pp. 2478–2490, 2009, doi: 10.3390/s90402478.

[9] N. L. Walker, A. B. Roshkolaeva, A. I. Chapoval, and J. E. Dick, “Recent advances in potentiometric biosensing,” Curr. Opin. Electrochem., vol. 28, p. 100735, 2021, doi: 10.1016/j.coelec.2021.100735.

[10] L. Manjakkal, B. Sakthivel, N. Gopalakrishnan, and R. Dahiya, “Printed flexible electrochemical pH sensors based on CuO nanorods,” Sensors Actuators, B Chem., vol. 263, pp. 50–58, 2018, doi: 10.1016/j.snb.2018.02.092.

[11] R. L. Mulvaney, “Chapter 38: Nitrogen-Inorganic Forms,” Methods Soil Anal. Part 3. Chem. Methods-SSSA B. Ser. 5, no. 5, pp. 1123–1184, 1996.

[12] L. Manjakkal, D. Szwagierczak, and R. Dahiya, “Progress in Materials Science Metal oxides based electrochemical pH sensors : Current progress and future perspectives,” no. February, 2019.

[13] F. F. Franco, L. Manjakkal, D. Shakthivel, and R. Dahiya, “ZnO based Screen Printed Aqueous Ammonia Sensor for Water Quality Monitoring,” Proc. IEEE Sensors, vol. 2019-Octob, pp. 1–4, 2019, doi: 10.1109/SENSORS43011.2019.8956763.

[14] E. Vinoth and N. Gopalakrishnan, “Fabrication of interdigitated electrode (IDE) based ZnO sensors for room temperature ammonia detection,” J. Alloys Compd., vol. 824, p. 153900, 2020, doi: 10.1016/j.jallcom.2020.153900.

[15] D. Punetha and S. K. Pandey, “Enhancement and Optimization in Sensing Characteristics of Ammonia Gas Sensor Based on Light Assisted Nanostructured WO3Thin Film,” IEEE Sens. J., vol. 20, no. 24, pp. 14617–14623, 2020, doi: 10.1109/JSEN.2020.3009661.

[16] S. Tohidi, M. Parhizkar, H. Bidadi, and R. Mohamad-Rezaei, “Electrodeposition of Polyaniline/Three-Dimensional Reduced Graphene Oxide Hybrid Films for Detection of Ammonia Gas at Room Temperature,” IEEE Sens. J., vol. 20, no. 17, pp. 9660–9667, 2020, doi: 10.1109/JSEN.2020.2991128.

[17] L. Manjakkal, I. P. Selvam, S. N. Potty, and R. S. Shinde, “Electrical and optical properties of aluminium doped zinc oxide transparent conducting oxide films prepared by dip coating technique,” Microelectron. Int., vol. 34, no. 1, pp. 1–8, 2017, doi: 10.1108/MI-06-2015-0058.

[18] P. Rong, S. Ren, Q. Yu, and D. Review, “Critical Reviews in Analytical Chemistry Fabrications and Applications of ZnO Nanomaterials in Flexible Functional Devices-A Review Fabrications and Applications of ZnO Nanomaterials in Flexible Functional,” vol. 8347, 2018, doi: 10.1080/10408347.2018.1531691.

[19] B. S. Kang, F. Ren, Y. W. Heo, L. C. Tien, D. P. Norton, and S. J. Pearton, “pH measurements with single ZnO nanorods integrated with a microchannel,” Appl. Phys. Lett., vol. 86, no. 11, pp. 1–3, 2005, doi: 10.1063/1.1883330.

[20] A. Wei, L. Pan, and W. Huang, “Recent progress in the ZnO nanostructure-based sensors,” Mater. Sci. Eng. B Solid-State Mater. Adv. Technol., vol. 176, no. 18, pp. 1409–1421, 2011, doi: 10.1016/j.mseb.2011.09.005.

[21] Z. Mwcnts et al., “Applied Surface Science Synthesis , characterization and gas sensing properties of,” Appl. Surf. Sci., vol. 413, no. 2, pp. 242–252, 2017, doi: 10.1016/j.apsusc.2017.03.290.

[22] R. Bhat and S. Sujatha, “Soil fertility and nutrient uptake by arecanut (Areca catechu L.) as affected by level and frequency of fertigation in a laterite soil,” Agric. Water Manag., vol. 96, no. 3, pp. 445–456, 2009, doi: 10.1016/j.agwat.2008.09.007.

[23] “Nonlinear Time Series Analysis - Holger Kantz, Thomas Schreiber - Google Books.” .

[Akshaya Kumar A]
Research Student
Date:
Place: Mangalagangothri

[Naveen Kumar S K]
Research supervisor